DOI: 10.1002/ejic.200700067

Dinuclear Nickel–Ruthenium Complexes as Functional Bio-Inspired Models of [NiFe] Hydrogenases

Yohan Oudart,[a] Vincent Artero,*[a] Jacques Pécaut,[b] Colette Lebrun,[b] and Marc Fontecave[a]

Keywords: Nickel / Ruthenium / Hydrogen / Electrocatalysis / Biomimetic chemistry / Hydrogenases

Three new dinuclear nickel ruthenium complexes, namely $[Ni(xbsms)Ru(p\text{-cymene})Cl]^+$, $[Ni(emi)Ru(CO)_2Cl_2]^{2-}$ and $[Ni(emi)Ru(p\text{-cymene})Cl]^-$ [H_2xbsms = 1,2-bis(4-mercapto-3,3-dimethyl-2-thiabutyl)benzene, H_2emi = *N*,*N*′-ethylenebis(2-mercaptoisobutyramide], have been synthesized and fully characterized as models of the active site of [NiFe] hydrogenases. The three-dimensional structure of $[Ni(xbsms)Ru(p\text{-cymene})Cl]^+$ reveals a nickel center in a square-planar dithioether-dithiolate environment that is connected to a ruthenium moiety via a $Ni(\mu\text{-}SR)_2Ru$ bridge. These complexes catalyze hydrogen evolution by electroreduction of the weakly acidic Et_3NH^+ ions in dimethylformamide and are therefore among the first bio-inspired functional models of [NiFe] hydrogenases. The catalytic activity of these new complexes is explained by the existence of a cooperative effect between the metal centers and is further related to their electronic properties.

Introduction

Hydrogenase enzymes catalyze the reversible formation/oxidation of dihydrogen and can be divided into two main classes, depending on their metal content.[1] In addition to classical Fe/S clusters, Fe-only hydrogenases display a hexanuclear active site (H-cluster) constituted by a [4Fe-4S] cluster bound through a cysteine-derived sulfur bridge to the $[Fe_2(\mu_2\eta^4\text{-}SRS)(CO)_3(CN)_2L]$ sub-site (R is proposed to be -CH_2NHCH_2-, L = H_2O, H_2 or H^-; Figure 1). By contrast, [NiFe] hydrogenases contain a dinuclear nickel-iron active center.[2] In the reduced active state the nickel ion is only coordinated by four cysteinate residues, two of which also bridge an organometallic {Fe(CO)$(CN)_2$} moiety (Figure 1). The [NiFe] hydrogenase from *Allochromatium vinosum* displays a Nernstian catalytic behavior for hydrogen oxidation when immobilized on a pyrolytic graphite "edge" electrode.[8] As unique molecular catalysts for H_2/H^+ interconversion, hydrogenases are thus competitive with platinum metal, which has prompted the synthesis, pioneered by Darensbourg et al., of a great variety of biomimetic complexes[9–11] with the aim of both better understanding the catalytic mechanism of native [NiFe] hydrogenases at the molecular level and developing new electrocatalysts to be used in fuel-cells for hydrogen uptake or in electrolytic/photosynthetic cells for hydrogen production. The most accurate of these structural mimics are $[(bdt)Ni(\mu_2\text{-}"S_3")Fe(CO)(PMe_3)_2]$ [H_2"S_3" = bis(2-mercaptophenyl)sulfide; H_2bdt = 1,2-benzenedithiol],[12] $[Ni(xbsms)Fe(CO)_2I_2]$ [H_2xbsms = 1,2-bis(4-mercapto-3,3-dimethyl-2-thiabutyl)-benzene],[13] and $[(dedtc)Ni(pdt)Fe(CO)_2(CN)_2]^-$ (dedtc$^-$ = diethyldithiocarbamato anion; H_2pdt = propanedithiol),[14] all of which have a nickel ion in an S_4 environment and CO ligands bound to iron (Figure 2). However, no catalytic activity has been reported so far for dinuclear nickel-iron complexes, and hydrogen evolution activity has only been demonstrated with trinuclear biomimetic complexes: $[(bdt)\{Ni(PMe_3)\}_2(bdt)_2Fe(CO)]$[15] stoichiometrically reduces HBF_4 to H_2 and $[Ni(L)Fe_2(CO)_6]$ [L = *S*,*S*′-bis(2-mercapto-5-methylphenyl)-1,4-dithiabutane] electrocatalyzes the reduction of CF_3COOH to H_2 at –1.64 V vs. Fc/Fc^+ in CH_2Cl_2.[16] In a bio-inspired approach, we recently

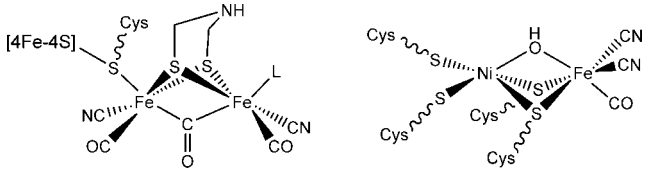

Figure 1. Structure of the active sites of iron-only hydrogenases in the oxidized state (left, L = H_2O, H_2 or H^-)[3,4] and [NiFe] hydrogenases in the Ni-B inactive ready state[5,6] (right, the bridging hydroxido ligand is not present in the reduced active states[7]).

[a] Laboratoire de Chimie et Biologie des Métaux; Université Joseph Fourier, CNRS UMR 5249, CEA, DSV/iRTSV/LCBM, Bâtiment K',
17 Rue des Martyrs, 38054 Grenoble Cedex 9, France
[b] Laboratoire de Reconnaissance Ionique et Chimie de Coordination, LCIB (UMR-E 3 CEA-UJF) DRFMC,
17 Rue des Martyrs, 38054 Grenoble Cedex 9, France

Supporting information for this article is available on the WWW under http://www.eurjic.org or from the author.

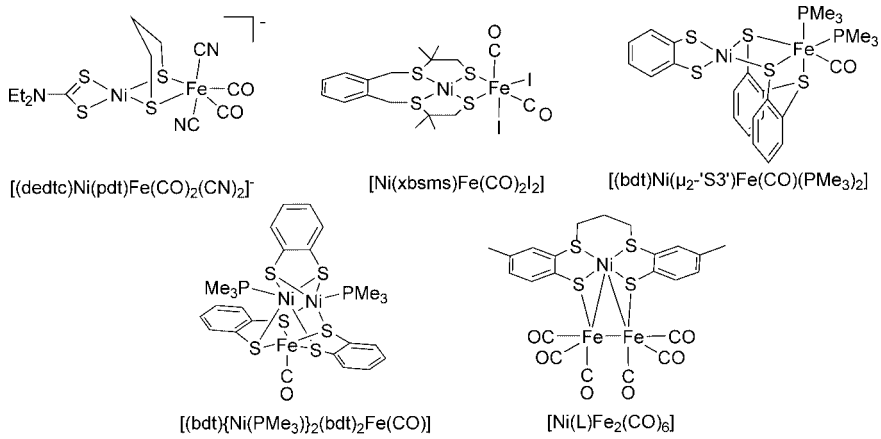

Figure 2. Selected structural models for [NiFe] hydrogenases from the literature (references are given in the text).

reported the catalytic activity of a dinuclear nickel-ruthenium complex in which an electron-rich organometallic moiety is introduced as a surrogate for the {Fe(CO)(CN)$_2$} fragment.[17] In order to shed light on the structure-function relationships in this class of catalysts, and to gain more insight into the reaction mechanism, we have prepared three new compounds that vary in both the tetradentate ligand around the nickel ion and the organometallic ligand set of the ruthenium center. Their catalytic activity for Et_3NH^+ reduction in dimethylformamide is investigated, and further comparison with the activity of structurally related mononuclear complexes of nickel and ruthenium provides evidence for a synergic effect between the metal centers in these dinuclear catalysts.

Results

Syntheses

Treatment of [Ni(xbsms)][18] with half an equivalent of [RuCl$_2$(*p*-cymene)$_2$]$_2$ in CH_2Cl_2 under argon afforded [Ni(xbsms)Ru(*p*-cymene)Cl]Cl (**1**Cl, Figure 3) in high yield, chromatographic purification of which yielded an analytically pure compound. Subsequent treatment with one equivalent of $AgBF_4$ in CH_2Cl_2 yielded **1**BF_4. This synthesis is very similar to that used previously for the preparation of [Ni(xbsms)Ru(CO)$_2$Cl$_2$] (**2**).[17]

Similarly, treatment of (NEt$_4$)$_2$[Ni(emi)] [H$_2$emi = *N*,*N*′-ethylenebis(2-mercaptoisobutyramide)][19] with half an equivalent of [RuCl$_2$(*p*-cymene)$_2$]$_2$ in CH_2Cl_2 under argon afforded (NEt$_4$)[Ni(emi)Ru(*p*-cymene)Cl] [(NEt$_4$)**3**, Figure 3]. (NEt$_4$)**3** can be purified by precipitation upon addition of pentane to a tetrahydrofuran solution even though samples proved to be systematically contaminated with Et_4NCl salt. The compound (NEt$_4$)$_2$[Ni(emi)Ru(CO)$_2$Cl$_2$] [(NEt$_4$)$_2$**4**, Figure 3] was obtained from the stoichiometric reaction of (NEt$_4$)$_2$[Ni(emi)] with [Ru(CO)$_2$Cl$_2$]$_n$ although it proved difficult to purify, the major impurities being Et_4NCl and (NEt$_4$)[Ni(emi)Ru(CO)$_3$Cl]. The latter arises from the reaction of (NEt$_4$)$_2$[Ni(emi)] with [Ru(CO)$_3$Cl$_2$], which often contaminates samples of [Ru(CO)$_2$Cl$_2$].

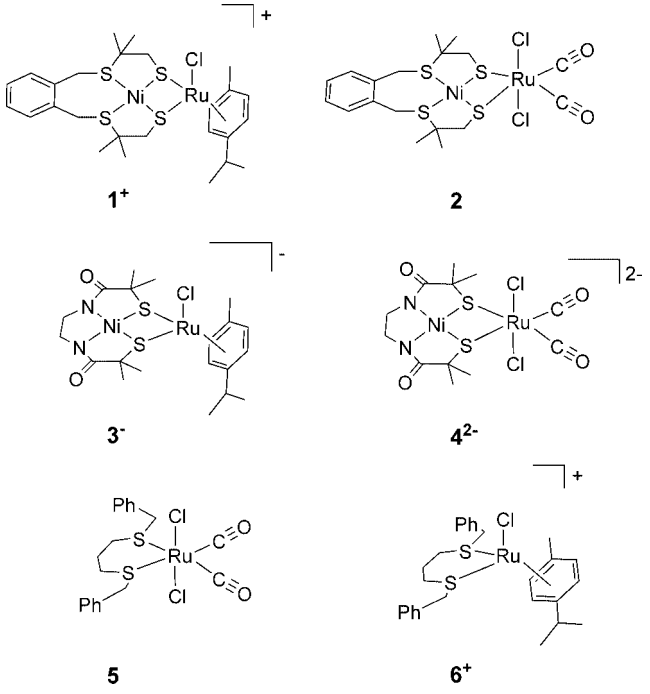

Figure 3. Molecular structures of the dinuclear nickel-ruthenium and mononuclear ruthenium complexes.

Two mononuclear ruthenium compounds, namely [("C_3S_2")Ru(CO)$_2$Cl$_2$] (**5**, Figure 3) and [("C_3S_2")RuCl(*p*-cymene)$_2$]Cl (**6**Cl, Figure 3) were also prepared by reaction of [Ru(CO)$_2$Cl$_2$]$_n$ and [RuCl$_2$(*p*-cymene)$_2$]$_2$ with 1,7-diphenyl-2,6-dithiaheptane ("C_3S_2"),[20] a bidentate ligand bearing two dithioether functions, in order to compare the dinuclear catalysts with mononuclear compounds having the same coordination sphere. Both complexes were purified by silica gel column chromatography to afford analytically pure powders.

Structures of [Ni(xbsms)Ru(p-cymene)Cl]BF_4 and [("C_3S_2")Ru(p-cymene)Cl]BF_4

The structure of the dinuclear cation **1**$^+$ in **1**BF_4 (Figure 4) is very similar to that of **2**,[17] with the *p*-cymene ligand replacing both the CO ligands and one chloride. Com-

plex $\mathbf{1}^+$ is furthermore structurally related to $[Ni(S_2N_2)Ru(arene)Cl]^+$ {arene = *p*-cymene or C_6Me_6; $S_2N_2^{2-}$ = $[S(CH_2)_2NMe(CH_2)]_2^{2-}$}, which was recently described by Rauchfuss et al.[21] The nickel atom is in a square-planar environment formed by the four sulfur atoms and the sulfur atoms of the thiolate groups are involved in two bridges with the ruthenium atom. Due to steric interactions with the axial methyl groups of the {Ni(xbsms)} fragment, the ruthenium moiety is located *trans* to the axial methyl groups and therefore *cis* to the aromatic cycle of the xbsms ligand.[22] A chloride ligand bound to ruthenium is directed towards, but does not interact with, the nickel atom [d(Cl···Ni) = 3.20 Å]. The ruthenium is in an octahedral environment and the nickel–ruthenium distance (3.29 Å) is longer than that in complex **2**, although both Ni–S [2.1692(15) and 2.1858(14) Å] and Ru–S [2.4020(14) and 2.4210(14) Å] bonds are only 0.02 Å shorter. This could be the consequence of a less-pronounced bending of the $Ni(\mu\text{-}S)_2Ru$ core (hinge angle 129.8° as compared to 124.1° in **2**). Significant distortion in the equatorial plane of the ruthenium octahedra arises from the acute S1–Ru–S4 angle [71.10(5)°] due to bridging constraints.

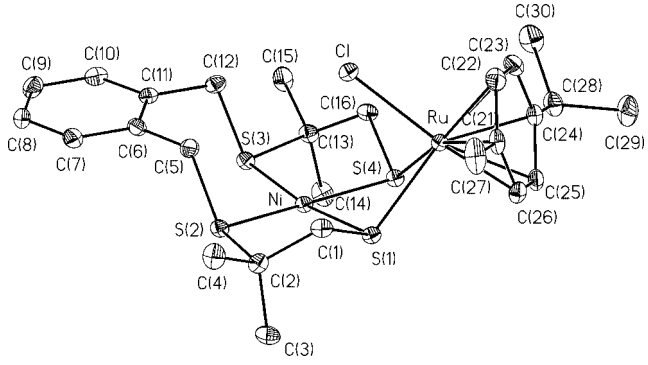

Figure 4. Structure of the cation $\mathbf{1}^+$ in $\mathbf{1}BF_4$ (30% probability thermal ellipsoids).

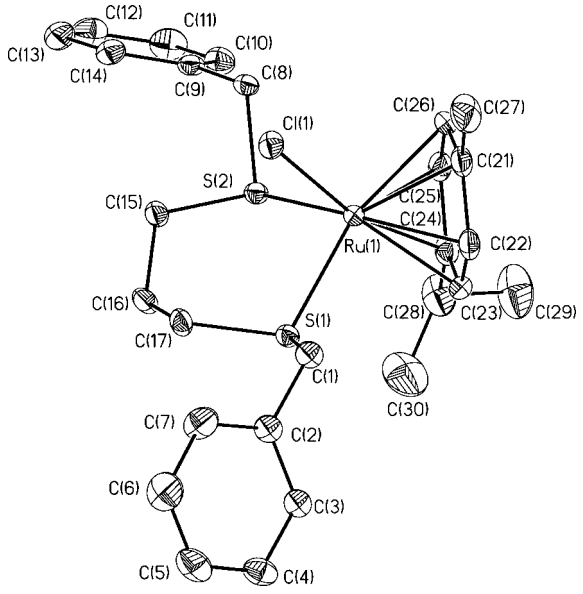

Figure 5. Structure of the cation $\mathbf{6}^+$ in $\mathbf{6}Cl{\cdot}2CH_2Cl_2$ (30% probability thermal ellipsoids).

The structure of complex $\mathbf{6}^+$ is shown in Figure 5. The ruthenium atom is in a pseudo-octahedral environment formed by the aromatic ligand, two thioether groups, and a chloride anion. The sulfur–ruthenium bonds [2.3737(11) and 2.3825(10) Å] are only slightly shorter than the ruthenium-thiolate bonds in $\mathbf{1}^+$, which means that $\mathbf{6}^+$ can thus be considered as a good comparative model for the ruthenium coordination sphere in $\mathbf{1}^+$.

Spectroscopic Characterization

Infrared Spectroscopy

The infrared spectra of **2**, $\mathbf{4}^{2-}$, and **5**, which have the same ruthenium moiety, display two ν_{CO} bands of equal intensity, in agreement with a *cis* arrangement of the carbonyl ligands at the ruthenium center (A_1 and B_1 stretching modes in C_{2v} symmetry). Extraction of the force constants k_{CO} (Figure 14) was done using the secular equations in the C_{2v} symmetry group.[23] As the C≡O force constant is directly related to the intensity of the metal-to-ligand π-backbonding, we were able to order all three compounds with regard to the electron richness of the ruthenium center and thus the electronic properties of their ligands. As expected, the dithioether ligand in complex **5** is less electron-donating than [Ni(xbsms)], which coordinates to ruthenium through its thiolate groups in complex **2**. $[Ni(emi)]^{2-}$ is the most electron-donating ligand in this series, probably due to its negative charge.

NMR Spectroscopy

The ^1H and ^{13}C NMR spectra of $\mathbf{1}^+$ indicate a C_s symmetry with heterotopic faces for the xbsms ligand. As 2D NMR correlation experiments correlate with crystallographic distances, the solid-state molecular structure is probably retained in solution, as previously reported for **2**.[17] The observation of two doublets (^3J = 5.7 and 6 Hz) for the aromatic protons of the *p*-cymene moiety in $\mathbf{1}^+$ and $\mathbf{3}^-$ indicates a free rotation around the ruthenium-arene bond. The ^1H NMR spectra of $(NEt_4)\mathbf{3}$ and $(NEt_4)_2\mathbf{4}$ display two singlets for the methyl and methylene groups of the emi^{2-} ligand, with chemical shifts different from the corresponding ones in the parent $[Ni(emi)]^{2-}$ complex. This suggests a symmetrical coupling of the nickel and ruthenium moieties. One singlet is masked by the signals of the Et_4N^+ cation but is clearly seen in the 2D ^1H-^{13}C spectra. Integration measurements are nevertheless in good agreement with the proposed charges of the complexes. A comparison of the chemical shifts for the aromatic protons in the organometallic moieties of $\mathbf{1}^+$, $\mathbf{3}^-$, and $\mathbf{6}^+$ establishes the same order as established above for the different ligands of ruthenium regarding their electron-donating properties.

Electrochemistry

The cyclic voltammograms recorded at a scan rate of 100 mV s^{-1} for complexes **5** and $\mathbf{6}^+$ in dimethylformamide

display one irreversible reduction wave at –1.29 V and –0.97 V vs. Ag/AgCl, respectively (see Supporting Information). Coulometry during bulk electrolysis experiments revealed that these waves represent a one-electron process and can thus be assigned to the reduction of Ru^{II} to Ru^{I}. Complex **5** is more difficult to reduce than $\mathbf{6}^{+}$ and thus the metal in the $\{Ru(CO)_2Cl_2\}$ moiety is more electron-rich than in $\{Ru(p\text{-cymene})Cl\}^{+}$.

The cyclic voltammogram of **1**Cl (Figure 6, trace a) in dimethylformamide shows a reversible electron-transfer process at +0.60 V vs. Ag/AgCl. This process has not yet been definitely assigned but we have evidence that the oxidation concerns the whole $\{Ni(\mu\text{-}S)_2Ru\}$ moiety. In addition, as in $[Ru(p\text{-cymene})Cl_2]_2$, the ruthenium center in **1**Cl displays a chemically irreversible one-electron reduction peak at –0.82 V with the corresponding anodic peak at –0.15 V. These features are consistent with an ECE mechanism (E = electron-transfer step; C = chemical step) involving the irreversible loss of a chloride ligand to yield a coordinatively unsaturated Ru^{I} species. Such a mechanism, although bielectronic, has previously been observed for *trans*(Cl)-$[Ru(bipy)(CO)_2Cl_2]$.[24] Furthermore, an irreversible one-electron process is observed at –1.42 V. This can be tentatively assigned to a nickel-centered reduction by comparison with the cyclic voltammogram of [Ni(xbsms)], which shows an irreversible cathodic peak at –1.45 V vs. Ag/AgCl in dimethylformamide (see trace a in Figure 9).

The cyclic voltammograms of (NEt_4)**3** (Figure 7, trace a) and $(NEt_4)_2$**4** (Figure 8, trace a) display a reversible wave at 0.24 V and 0.39 V vs. Ag/AgCl, respectively. The cyclic

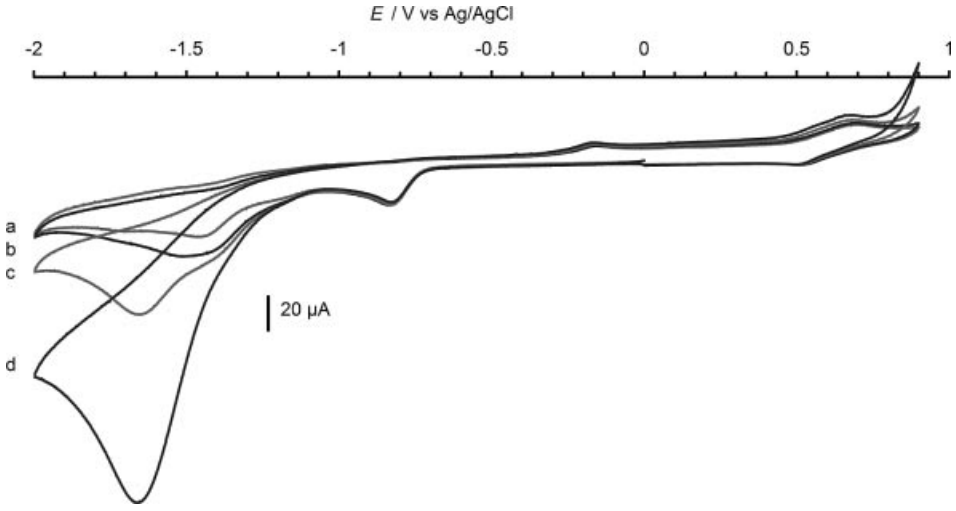

Figure 6. Cyclic voltammograms of **1**Cl (1.0 mM) in the presence of various amounts of Et_3NHCl recorded in a dimethylformamide solution of $n Bu_4NBF_4$ (0.1 M) on a glassy carbon electrode at 100 mV s^{-1}: a) 0 equiv.; b) 1.5 equiv.; c) 3.0 equiv.; d) 10 equiv.

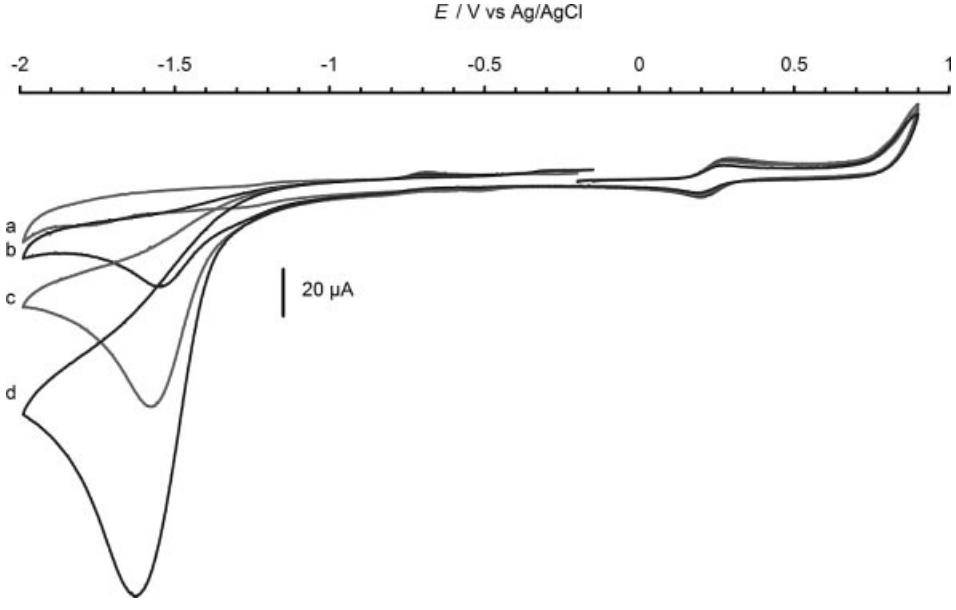

Figure 7. Cyclic voltammograms of (NEt_4)**3** (1.0 mM) in the presence of various amounts of Et_3NHCl recorded in a dimethylformamide solution of $n Bu_4NBF_4$ (0.1 M) on a glassy carbon electrode at 100 mV s^{-1}: a) 0 equiv.; b) 1.5 equiv.; c) 3.0 equiv.; d) 10 equiv.

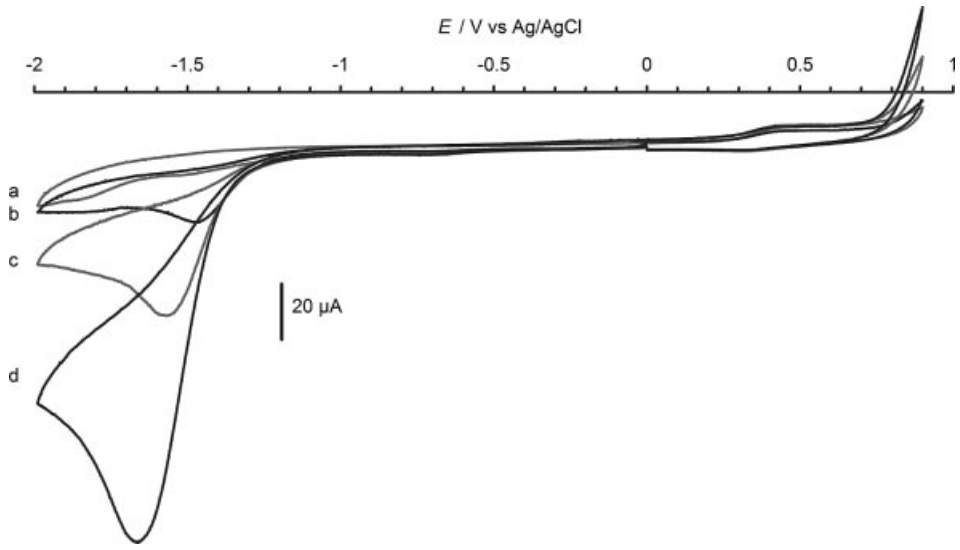

Figure 8. Cyclic voltammograms of $(NEt_4)_2$**4** (1.0 mM) in the presence of various amounts of Et_3NHCl recorded in a dimethylformamide solution of nBu_4NBF_4 (0.1 M) on a glassy carbon electrode at 100 mV s^{-1}: a) 0 equiv.; b) 1.5 equiv.; c) 3.0 equiv.; d) 10 equiv.

voltammogram of (NEt_4)**3** exhibits two cathodic irreversible and flattened waves at –1.30 and –1.85 V vs. Ag/AgCl, which were shown to be monoelectronic by coulometric experiments. An irreversible anodic peak is seen at –0.66 V vs. Ag/AgCl on the reverse scan. As for **1**Cl, an ECE mechanism involving loss of a chloride ligand from the ruthenium center can be proposed. $(NEt_4)_2$**4** is also monoelectronically and irreversibly reduced at –1.54 V vs. Ag/AgCl, although no anodic peak can be observed in the reverse scan.

Proton Reduction Electrocatalysis

Cyclic Voltammetry

Addition of increasing amounts of Et_3NHCl to dimethylformamide solutions of **1**Cl (Figure 6), (NEt_4)**3** (Figure 7), or $(NEt_4)_2$**4** (Figure 8) leads to the appearance of an electrocatalytic wave corresponding to hydrogen evolution, which increases in height and shifts to lower potentials. The peak potentials of the electrocatalytic waves as a function of the number of equivalents of acid added, which range from –1.46 to –1.57 V vs. Ag/AgCl, are listed in Table 1. The appearance of this electrocatalytic wave is the only observed modification of the cyclic voltammogram upon addition of acid, which suggests that these complexes are not prone to protonation in the Ni^{II}-Ru^{II} state. In the cases of **1**Cl and (NEt_4)**3**, the electrocatalytic wave is a new cathodic process that occurs after an irreversible reduction step. A similar behavior has already been observed for **2**.[17] As far as $(NEt_4)_2$**4** is concerned, the electrocatalytic wave develops on the irreversible cathodic process observed at –1.54 V vs. Ag/AgCl in the absence of acid.

The nickel precursor [Ni(xbsms)] also catalyzes the hydrogen evolution reaction from Et_3NHCl at –1.45 V vs. Ag/AgCl in dimethylformamide (Figure 9). The electrocatalytic behavior in this case consists of the appearance of a new wave at –1.35 V vs. Ag/AgCl upon addition of one equivalent of Et_3NH^+. This wave increases in height and shifts to lower potential upon further addition of acid.

$(NEt_4)_2$[Ni(emi)] is not stable in the presence of Et_3NHCl in dimethylformamide, as revealed by the formation of a black precipitate. We suspect that a disproportionation reaction takes place after protonation of $[Ni^{II}(emi)]^{2-}$ to produce a Ni^{III} species together with elemental nickel. The resulting mixture catalyzes Et_3NHCl electroreduction, poss-

Table 1. Electrocatalytic properties of **1**Cl, **2**, (NEt_4)**3**, $(NEt_4)_2$**4**, [Ni(xbsms)], and $(NEt_4)_2$[Ni(emi)]. Electrocatalytic peak potentials (E_{her}, V) were determined by cyclic voltammetry at 100 m V s^{-1} in a dimethylformamide solution of nBu_4NBF_4 (0.1 M) on a glassy carbon electrode. TOF and total TON were determined by bulk electrolysis experiments at –1.60 V of a dimethylformamide solution (6 mL) of nBu_4NBF_4 (0.1 M) and Et_3NHCl (0.5 mmol) at a mercury pool (1.23 cm^2) in the presence of millimolar concentrations of catalyst. All potentials are quoted with respect to Ag/AgCl.

	1Cl	**2**	(Et_4N)**3**	$(Et_4N)_2$**4**	[Ni(xbsms)]	$(Et_4N)_2$[Ni(emi)]
E_{her} with 1.5 equiv. of Et_3NHCl	–1.57	–1.59	–1.55	–1.46	–1.45	–
E_{her} with 3 equiv. of Et_3NHCl	–1.65	–1.66	–1.60	–1.57	–1.46	–
E_{her} with 10 equiv. of Et_3NHCl	–1.66	–1.78	–1.64	–1.67	–1.52	–
Total TON after 4.5 h	28.9	12.4	26.5	6.8	6.4	5.5
TOF [h^{-1}]	6.4	2.75	5.9	1.5	1.4	1.2
TON during the first hour of electrolysis (= TOF)	5.4	3.5	7.75	2.3	2	1.2

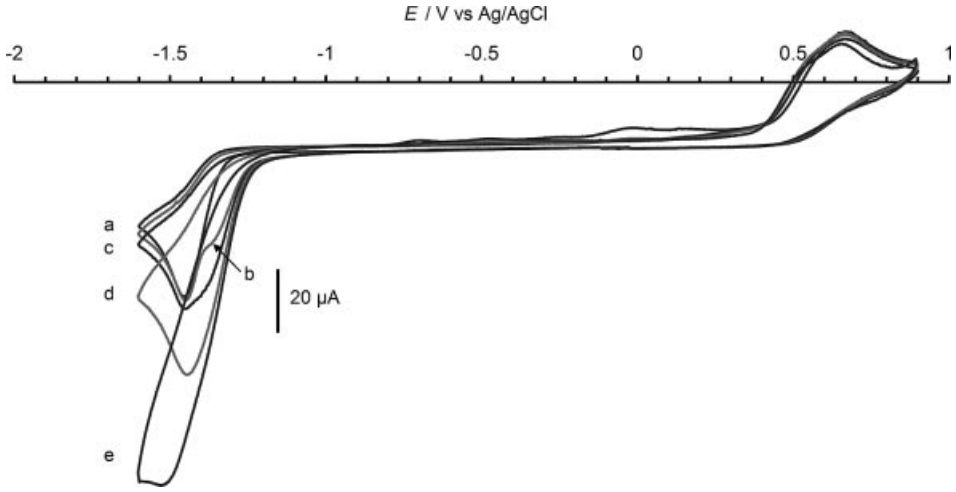

Figure 9. Cyclic voltammograms of [Ni(xbsms)] (1.0 mM) in the presence of various amounts of Et_3NHCl recorded in a dimethylformamide solution of nBu_4NBF_4 (0.1 M) on a glassy carbon electrode at 100 mV s^{-1}: a) 0 equiv.; b) 1.0 equiv.; c) 1.5 equiv.; d) 3.0 equiv.; e) 10 equiv.

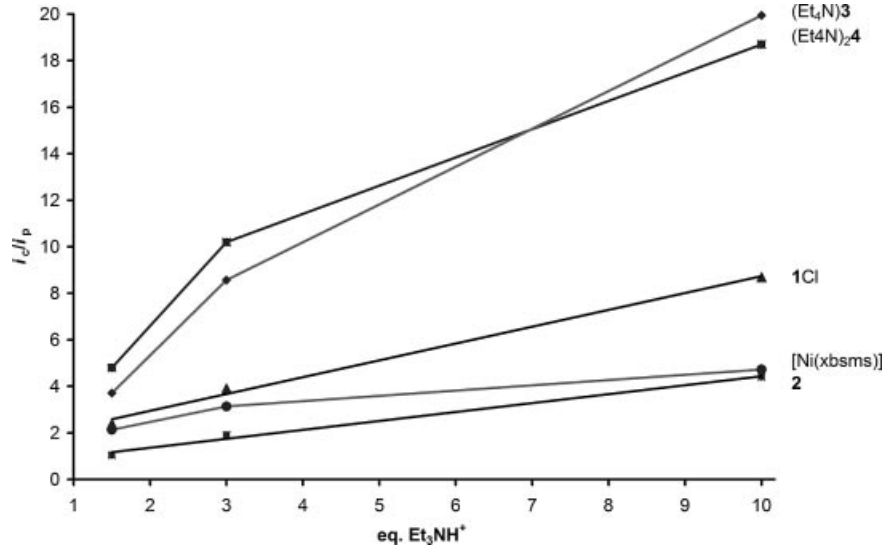

Figure 10. Evolution of the i_c/i_p ratio between the catalytic peak current and the current of a monoelectronic wave as a function of the number of equivalents of acid added for **1**Cl, **2**, (NEt_4)**3**, $(NEt_4)_2$**4**, and [Ni(xbsms)].

ibly due to heterogeneous catalysis by elemental nickel, as shown by the appearance of an electrocatalytic wave with peak maxima below –1.7 V vs. Ag/AgCl in the cyclic voltammograms (see Supporting Information).

In contrast, the mononuclear ruthenium complex **6**Cl does not exhibit electrocatalytic activities. As far as complex **5** is concerned, some electrocatalytical activity is observed at potentials below –1.8 V vs. Ag/AgCl. Thus, for millimolar solutions of **5** in the presence of 10 equivalents of Et_3NHCl, the reduction current between –1.8 and –2.0 V vs. Ag/AgCl is higher than that observed by direct reduction at the electrode in the absence of catalyst (see Supporting Information).

Figure 10 shows the evolution of the i_c/i_p ratio, where i_c is the catalytic peak current and i_p the peak current of a monoelectronic wave, as a function of the number of equivalents of acid added. It is clear that the {Ni(emi)}-based catalysts have much higher catalytic peak intensities than the {Ni(xbsms)}-based catalysts. This reveals that the {Ni(emi)} moiety enhances the catalytic rate. It also appears that the evolution of the catalytic peak current for **1**Cl and **2** is proportional to the number of equivalents of added acid, which could indicate that the rate-determining step is a protonation.

Modeling Cyclic Voltammograms

In order to characterize the mechanisms for hydrogen production, we modeled the cyclic voltammograms for the electroreduction of Et_3NH^+ catalyzed by **2** and $(NEt_4)_2$**4** in dimethylformamide using the DigiElch software.[25–30] Proton reduction yields dihydrogen following two general pathways depending on whether the H–H bond is formed in a homolytic or a heterolytic step.[31] The general mechanistic schemes are given in Scheme 1. Both pathways include pro-

tonation of the metal center to give a metal hydride complex. In the homolytic mechanism, H_2 evolution results from a reductive elimination reaction from two metal hydride moieties, whereas in the heterolytic pathway the metal hydride species is subjected to proton attack, which results in hydrogen production. We were unable to model the experimental cyclic voltammograms, namely to reproduce high i_c/i_p ratios, using the homolytic hydrogen formation mechanism. This could be due to the fact that the rate of a step which is second-order with regard to the catalyst is necessarily slow and thus makes the homolytic pathway less kinetically favorable than the heterolytic one. In the following we will therefore only consider the heterolytic pathway.

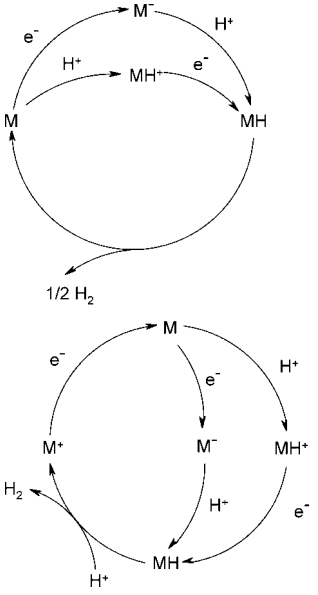

Scheme 1. Homolytic (top) and heterolytic (bottom) pathways for proton reduction catalyzed by a coordination compound.

The relative order of the two one-electron transfer and two protonation steps in the mechanism can be immediately determined by a simple examination of the voltammograms. In the cases of **1**Cl, **2**, and (NEt_4)**3**, the electrocatalytic wave develops at potentials more negative than the reduction potential of the catalyst; this implies that the hydride moiety formed by protonation after reduction of the catalyst needs to be activated by further reduction. The ECEC mechanism used for simulation of the electrocatalytic behavior of **2** is shown in Scheme 2. By contrast, the development of an electrocatalytic wave on a reduction wave of the catalyst, as

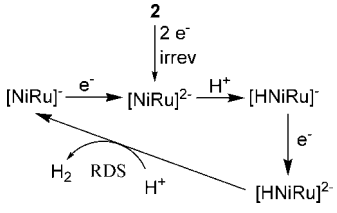

Scheme 2. Catalytic ECEC mechanism used for modeling the electrocatalytic behavior of **2** (RDS indicates the rate-determining step).

in the case of $(NEt_4)_2$**4**, suggests that the two one-reduction steps occur before the two protonation steps. Scheme 3 shows the suggested ECCE mechanism for this complex.

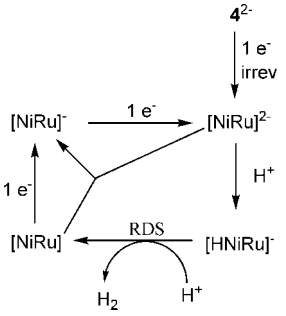

Scheme 3. Catalytic ECCE mechanism used for modeling the electrocatalytic behavior of $(NEt_4)_2$**4** (RDS indicates the rate-determining step).

The charge-transfer parameters (E^0, a, k_s) and diffusion coefficients describing the redox properties of the catalysts were determined from voltammograms obtained in the absence of acid and then used as such for simulation in the presence of acid. Heterogeneous charge-transfer processes are relatively slow, with rate constants k_s ranging from 10^{-3} to 10^{-2} cm s^{-1}. Total and fast chemical reactions were introduced into the model to account for the irreversibility of the electrochemical processes.

By including the catalytic steps shown in Schemes 2 and 3 we succeeded in modeling the experimental cyclic voltammograms (Figures 11 and 12) and were able to reproduce the experimental data recorded at variable scan rates in the presence of a 1/1.5-, 3-, and 10-fold molar excess of Et_3NHCl with one set of thermodynamic and kinetic constants for each compound. We chose the height, position, and shape of the catalytic wave as relevant criteria for the evaluation of the simulations. As can be seen in Figures 11 and 12, the major difference between simulated and experimental values concerns the reverse scan. In the case of $(NEt_4)_2$**4**, a disproportionation reaction was introduced to better reproduce the reverse scan of the electrocatalytic wave. Its equilibrium constant was calculated from the standard potentials of the corresponding redox couples and the scan rate was set as being diffusion-controlled.

The second protonation step was found to be the rate-determining step in both cases since the value of its rate constant [10^3 mol^{-1} L s^{-1} for **2** and 10^4 mol^{-1} L s^{-1} for $(NEt_4)_2$**4**] determines the height of the electrocatalytic wave.

Bulk Electrolysis Experiments

As for **2**, hydrogen evolution was detected and quantified by gas chromatography and volumetry during bulk electrolysis experiments of Et_3NHCl on a mercury pool at –1.60 V vs. Ag/AgCl in dimethylformamide with **1**Cl, (NEt_4)**3**, $(NEt_4)_2$**4**, and [Ni(xbsms)] as electrocatalysts. As an example, Figure 13 shows the evolution of the charge passed during the bulk electrolysis of 0.5 mmol of Et_3NHCl in the presence of 5 μmol of **1**Cl. The correlation between the charge and volume of evolved hydrogen is shown in the

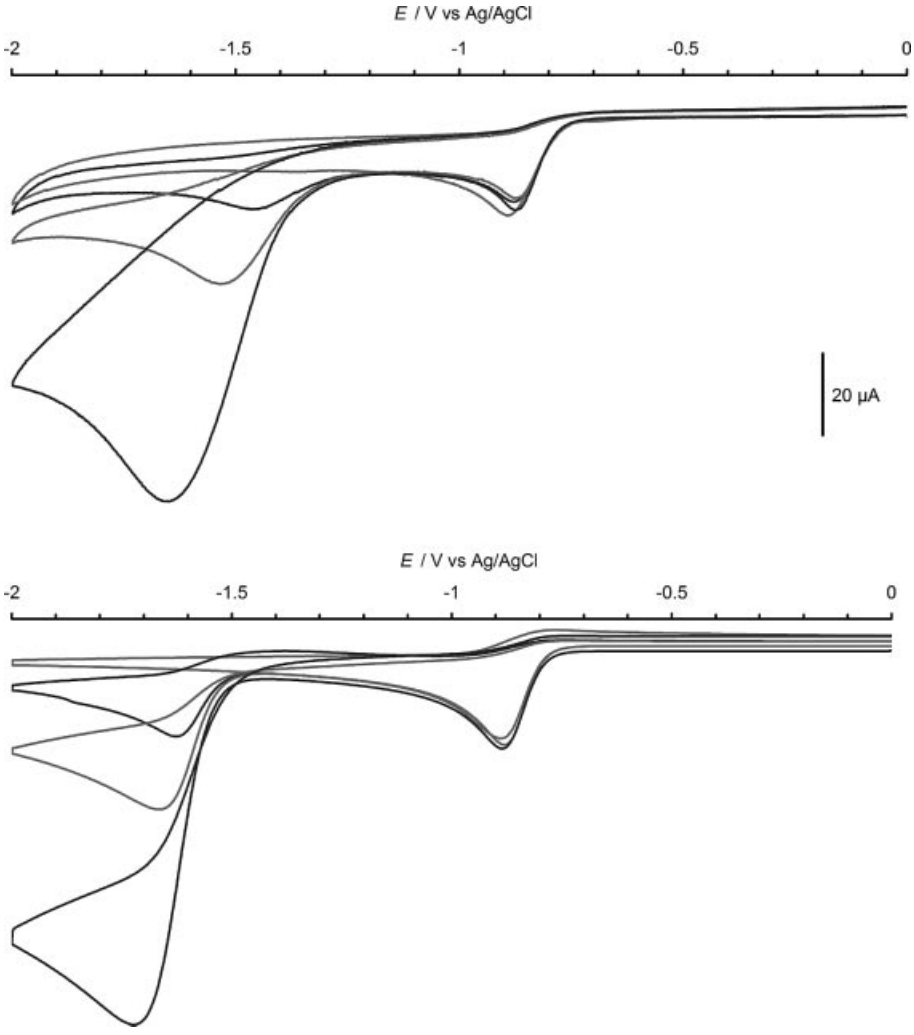

Figure 11. Experimental (top) and simulated (bottom) cyclic voltammograms of **2** (1.0 mM) recorded in a dimethylformamide solution of nBu$_4$NBF$_4$ (0.1 mM) at a glassy carbon electrode in the presence of Et$_3$NHCl (1.0, 3.0, and 10 equiv.). Scan rate: 100 mV s^{-1}.

inset. The faradaic yield reaches 98%. Et$_3$NHCl is quantitatively converted to H_2 (50 turnovers) in 4 h [maximum turnover frequency (TOF_{max}) of 22 h^{-1}]. Addition of a further 0.5 mmol of Et$_3$NHCl allowed a second electrolytic run, with comparable yield and slightly lower rate, thereby indicating the chemical stability of the catalyst.

Table 1 summarizes the catalytic parameters of the various compounds, including complex **2**, determined under the same conditions and in the same electrolysis cell with a mercury pool of smaller but reproducible area. All of the dinuclear complexes catalyze Et$_3$NHCl reduction faster than their corresponding nickel precursor and all except (NEt$_4$)$_2$**4** are more active than [Ni(xbsms)]. The {Ru(*p*-cymene)Cl}$^+$ derivatives **1**Cl and (NEt$_4$)**3** are clearly the most efficient catalysts during bulk electrolysis experiments. Complexes **5** and **6**Cl are totally inactive under these conditions at –1.6 V vs. Ag/AgCl.

Finally, in order to compare the catalysts in terms of their chemical stability during cycling, we recorded cyclic voltammograms and/or steady-state rotating-disk-electrode voltammograms for the oxidative process before and after catalysis. Whereas the anodic wave disappears completely after 15 turnovers for catalysts **1**Cl and **2**, complexes (NEt$_4$)**3** and (NEt$_4$)$_2$**4** are quite stable under the catalytic conditions since the oxidative process appears quite unaffected after 29 and 27 turnovers, respectively (see Supporting Information).

Discussion

The rational synthesis of heterodinuclear complexes that model the active sites of [NiFe] hydrogenases is a promising but challenging approach to the design of new catalysts for H_2 production or activation.[31] As far as nickel thiolate complexes are concerned, the main difficulty resides in the control of the nuclearity of the synthetic compound. The use of chelating ligands serves to avoid the formation of homometallic nickel clusters and a careful design of the precursor for the second metal site is required to avoid the formation of heterometallic oligomers. In particular, this implies that only a few labile ligands can be present on this

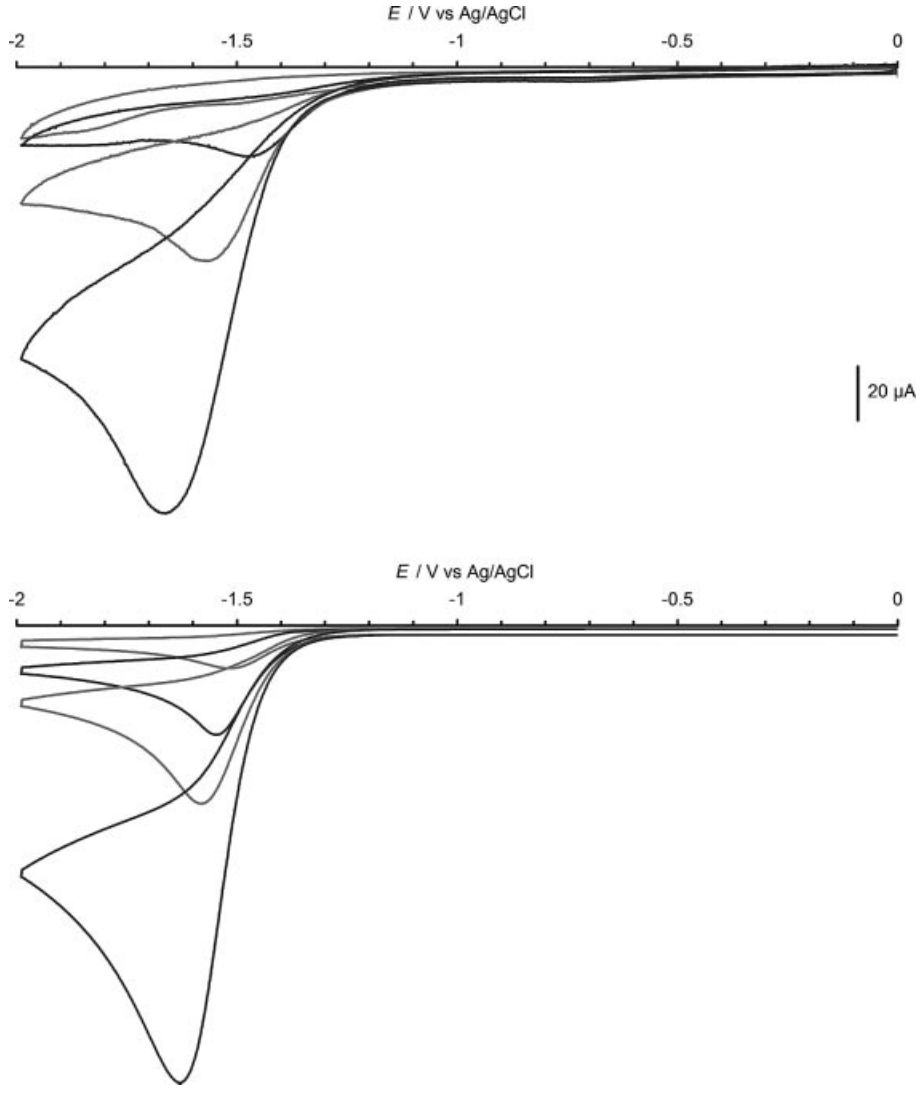

Figure 12. Experimental (top) and simulated (bottom) cyclic voltammograms of $(NEt_4)_2$**4** (1.0 mM) recorded in a dimethylformamide solution of nBu$_4$NBF$_4$ (0.1 M) at a glassy carbon electrode in the presence of Et$_3$NHCl (1.5, 3.0, and 10 equiv.)). Scan rate: 100 mV s^{-1}.

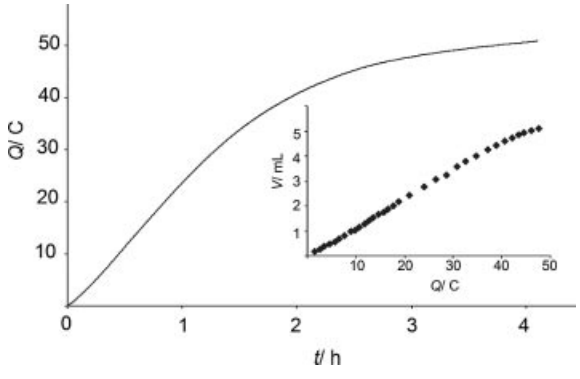

Figure 13. Coulometry for bulk electrolysis at –1.60 V vs. Ag/AgCl of a dimethylformamide solution (10 mL) of Et$_3$NHCl (0.05 M) and nBu$_4$NBF$_4$ (0.1 M) at a mercury pool (approx. 3 cm^2) in the presence of **1**Cl (0.5 mM). The volume of hydrogen evolved as a function of charge is represented in the inset.

precursor. However, as a consequence, most of the reported models display a coordinatively saturated coordination sphere around the iron center with consequent low reactivity. Exceptions for nickel-iron assemblies are found for [Ni(xbsms)Fe(CO)$_2$I$_2$],[13] which contains labile iodide ligands, and [Ni(S{(CH$_2$)$_2$NMe(CH$_2$)$_2$S}$_2$)FeCp]$^+$,[32] which displays a vacant coordination site at the iron center. Unfortunately, no reactivity study regarding proton reduction or hydrogen oxidation has been reported either for these two complexes or for the other dinuclear nickel-iron complexes described to date. This may be due to some inherent instability of these complexes upon redox switching during catalysis. We thus decided to substitute iron for the heavier metal ruthenium with the aim of isolating species stable enough for the observation of electrochemical catalysis of hydrogen production. This approach initially allowed the preparation of **2** and we report here the synthesis and characterization of three novel nickel-ruthenium heterodinu-

clear complexes carrying labile chloride ligands at the ruthenium metal center. In each case, the desired complex is the sole product of the reaction and separation from the salts is the sole purification step required. All four complexes contain the $\{Ni(\mu\text{-}SR)_2Ru\}$ fragment with bidentate coordination of the nickel complex to the ruthenium center. The hinge angles in **2** and $\mathbf{1}^+$ are in the range usually found in naturally occurring hydrogenases,[32] and the nickel–ruthenium distances are similar to the longer Ni–Fe distances observed in enzymes by X-ray crystallography: most of the nickel–iron distances determined for hydrogenases lie between 2.53 and 2.97 Å, which indicates some direct electronic interaction between the two metal centers, although, as an exception, a Ni–Fe distance of 3.23 Å was observed for the [NiFe] hydrogenase from *Desulfovibrio desulfuricans*.[33] However, computational modeling predicts large variations of this bond length in the active site depending on the redox state of the enzyme.[34]

Activation Potential

All three new nickel-ruthenium compounds synthesized exhibit electrocatalytic activity for hydrogen production with overvoltages (also called activation potential: the difference between the electrocatalytic potential and the equilibrium potential of the H^+/H_2 couple under the same conditions) of 0.8–1.0 V, as estimated from the tabulated value of –1.31 V vs. Fc/Fc^+ for the Et_3NH^+/H_2 couple in dimethylformamide.[35] There is no net benefit in substituting either arene for CO ligands on ruthenium or emi^{2-} for $xbsms^{2-}$ around the nickel ion as regards overvoltage.

For comparison, a variety of square-planar nickel complexes are known to catalyze proton electroreduction, most of which have an N_4 coordination sphere with mixed amino, imino, or pyridine ligands assembled in a macrocycle.[36–39] Except for $[Ni(L_{N4})]^+$ $\{L_{N4}^- = 2,6\text{-}HN[(CH_2)_3N{=}C(CH_3)]_2\text{-}C_5H_3N^-\}$, which is active at –1.1 V vs. SCE in acidic (pH 2) aqueous solution,[38] all of these catalysts are active at –1.5 to –1.6 V vs. SCE towards relatively weak acids or in neutral aqueous solutions. Two functional bio-inspired catalysts, namely $[(bdt)\{Ni(PMe_3)\}_2Fe(CO)(bdt)_2]$,[15] which stoichiometrically reduces HBF_4 into H_2, and $[Ni(L)\text{-}Fe_2(CO)_6]$ $[L = (CH_3C_6H_3S_2)_2(CH_2)_3]$, which electrocatalyzes the reduction of CF_3COOH into H_2 at –1.64 V vs. Fc/Fc^+ in CH_2Cl_2, were described recently.[16] All these complexes catalyze proton electroreduction with an activation potential of 0.8 to 1.2 V. Very recently, DuBois et al. have described a series of nickel bis(diphosphane) complexes that are very competitive, as regards electrocatalytic potential, as electrocatalysts for both proton reduction and hydrogen oxidation.[40,41] However, the unique catalytic properties of these new catalysts are due to the presence of pendant basic sites and are not directly related to the nature of the coordination sphere around nickel [amino residues located on the ligands play the role of proton relays and greatly enhance the activity relative to classical noncatalytic nickel bis(diphosphane) complexes].

Catalytic Rate and Stability

As seen in Figure 10, both (NEt_4)**3** and $(NEt_4)_2$**4** show high catalytic peak current enhancement relative to **1**Cl and **2**. Even though no direct analytical relationship between the catalytic peak current measured by cyclic voltammetry and turnover frequency exists, a comparison of the cyclic voltammograms recorded under the same conditions shows that the catalytic rate is greatly enhanced by the introduction of the emi^{2-} anion as a ligand in place of $xbsms^{2-}$.

The same considerations based on i_c/i_p values lead to the conclusion that the presence of an arene ligand rather than carbonyl ligands on the ruthenium center improves the efficiency of the catalyst. This is further confirmed by bulk electrolysis experiments: thus, when substituting $\{(p\text{-cymene})RuCl\}^+$ for $\{Ru(CO)_2Cl_2\}$ the rate of hydrogen production in both the {Ni(emi)} and {Ni(xbsms)} series is improved (Table 1).

Catalysis always takes place on or after an irreversible wave so that the isolated and structurally characterized dinuclear species are likely to be pre-catalysts rather than active catalysts. The exact nature of the chemical reaction following reduction is unknown. Loss of chloride ligand from the ruthenium center is likely, although radical reactions involving hydrogen atoms in the β-position with regards to the nickel center, as identified in mononuclear nickel thiolate complexes,[42] cannot be ruled out. Furthermore, no evidence for any breakdown of the dinuclear species could be obtained, and we could demonstrate that $\mathbf{3}^-$ and $\mathbf{4}^{2-}$ do not decompose during catalysis.

Cooperativity Between Metal Centers

The electrocatalytic properties of dinuclear complexes for hydrogen production clearly denote the existence of a cooperative effect between nickel and ruthenium. Thus, while $(NEt_4)_2$[Ni(emi)] and **5** or $\mathbf{6}^+$ display no or only weak catalytic activity (e.g. at potentials below –1.8 V vs. Ag/AgCl and with low turnover frequencies) the dinuclear catalysts (NEt_4)**3** and $(NEt_4)_2$**4** readily catalyze Et_3NHCl reduction near –1.6 V vs. Ag/AgCl, and hydrogen evolution during bulk electrolysis experiments at –1.6 V vs. Ag/AgCl is five times faster in the presence of (NEt_4)**3** than in the presence of $(NEt_4)_2$[Ni(emi)]. As for the [Ni(xbsms)] derivatives, coupling with ruthenium moieties results in an enhancement of the rate of hydrogen evolution by a factor of two (complex **2**) or five (complex **1**Cl). However, this is at the expense of the electrocatalytic potential, which is about 200 mV more negative than the electrocatalytic potential of [Ni(xbsms)] under the same conditions. Such a cooperative effect has been suggested to account for the higher activity of $[Ni_2(bis\text{-}cyclam)]^{4+}$ compared to $[Ni(cyclam)]^{2+}$ for proton reduction[37] and for the high activity in photoelectrochemical production of hydrogen catalyzed by bis(metallocene)s such as [1.1]ferrocenophane.[43]

Figure 14 shows the inverse correlation between the electrocatalytic potential and the C≡O force constant as a probe of the electron density on the metal centers for the three CO-containing compounds in this study. The nickel-iron hydrogenase from *D. gigas* nicely fits in this correlation

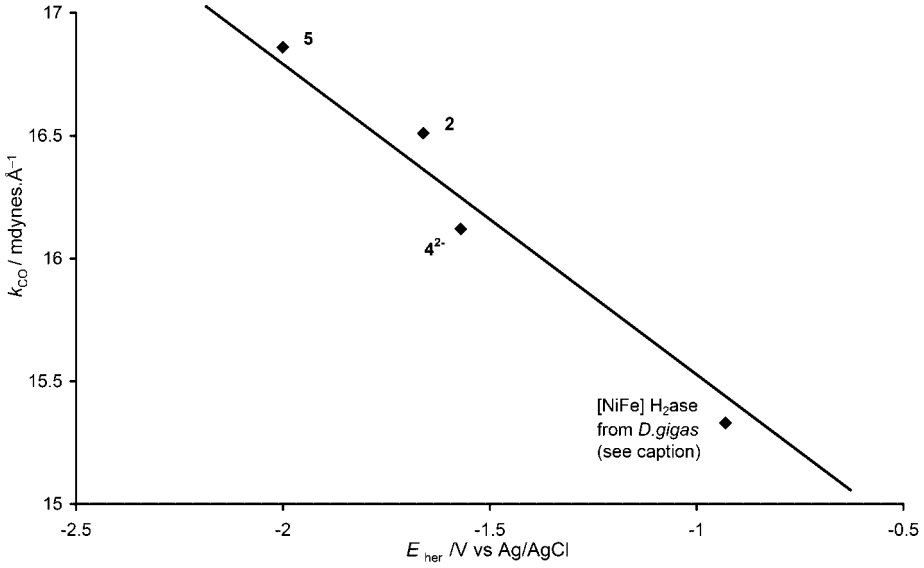

Figure 14. Correlation between the C≡O force constant (k_{CO}) and the electrocatalytic potential (E_{her}) for compounds **2**, $(NEt_4)_2$**4**, and **5**. Data have been extrapolated for [NiFe] hydrogenase from *D. gigas* in dimethylformamide solution using the measured ν_{CO} frequency for native enzyme in water and the experimental potential for reduction of Et_3NHCl on a platinum electrode in dimethylformamide.[35]

when extrapolating the redox potential measured in water to dimethylformamide solution. We can conclude from this correlation that the more electron-rich the metal center the better the catalyst as far as overvoltage is concerned. This implies that the rate-determining step has a nucleophilic nature and may involve a protonation. This is further supported, in the case of **1**Cl and **2**, by the relative linearity of the i_c/i_p ratio as a function of the number of equivalents of added acid and by modeling studies of the cyclic voltammograms of **2** and $(NEt_4)_2$**4**.

Modeling of the voltammograms was possible with classical catalytic mechanisms involving metal hydride species[44] resulting from the interaction of protons with the reduced dinuclear complexes. Two distinct mechanisms have been identified: $\mathbf{1}^+$, **2**, and $\mathbf{3}^-$ catalyze proton reduction by an ECEC mechanism similar to that (Scheme 3) proposed for proton electroreduction catalyzed by a rhodium porphyrin[45] and the $\{BF_2\}$-bridged cobaloxime $[Co(dmgBF_2)_2L_2]$ (L = H_2O, CH_3CN, dmf).[46] In contrast, $\mathbf{4}^{2-}$-catalyzed hydrogen evolution proceeds by an ECCE pathway similar to the catalytic mechanism for hydrogen evolution determined for iron porphyrin[47] or cobaloxime complexes.[48] The rate-determining step was found to be protonation of the hydride intermediate in both cases, as previously reported for iron porphyrin[47] or cobaloxime complexes.[48]

Conclusions

We have synthesized a series of novel bio-inspired dinuclear nickel-ruthenium complexes that are efficient catalysts for proton reduction under quite neutral conditions in dimethylformamide and have found evidence for a cooperative effect between the metal centers which enhances the catalytic rate, whereas high electron density at the metal centers favors low overvoltages. The catalysts are more stable when no hydrogen atom is present in the β-position with regard to the nickel center. These general trends may help in the synthesis of new catalysts with a lower overvoltage and higher stability.

Experimental Section

Materials: All reactions were carried out under argon using standard Schlenk techniques. Solvents were distilled under argon. NMR solvents were deoxygenated by three freeze-pump-thaw cycles and stored over molecular sieves. Commercial dimethylformamide and acetonitrile for electrochemistry were degassed by bubbling nitrogen through them. $(NEt_4)_2$[Ni(emi)],[19] [Ru(*p*-cymene)$Cl_2]_2$,[49,50] $[Ru(CO)_2Cl_2]_n$,[51,52] [Ni(xbsms)],[18] and 1,7-diphenyl-2,6-dithiaheptane ("C_3S_2")[20] were prepared according to reported procedures. The supporting electrolyte (nBu$_4$N)BF_4 was prepared from (nBu$_4$N)HSO_4 (Aldrich) and $NaBF_4$ (Aldrich) and dried overnight at 80 °C under vacuum. Triethylammonium chloride (Acros) was used as received.

Methods and Instrumentation: ^{1}H NMR spectra were recorded at room temperature in 5-mm tubes with a Bruker AC300 spectrometer equipped with a QNP probehead. ^{1}H NMR signals were assigned by NOE difference experiments performed using standard pulse sequences. IR spectra were recorded with a Bruker Vector 22 spectrophotometer (400–4000 cm^{-1}, Class 3A laser). The spectra were recorded in solution, using a KBr cell. UV/Vis spectra were recorded with a Carry Bio1 (Varian) spectrophotometer in quartz Schlenk cells. ESI mass spectra were recorded with a Finnigan LCQ thermoquest ion-trap. Elemental analyses were performed by the Service Central d'Analyse of the CNRS (Vernaison, France). All electrochemical measurements were carried out under nitrogen in a thermostatted cell at 20 °C. A standard three-electrode configuration was used consisting of a glassy carbon (3 mm in diameter) or platinum (2 mm in diameter) disk as the working electrode, an auxiliary platinum wire and an Ag/AgCl/aqueous $AgCl_{sat}$ + KCl

3 M (named Ag/AgCl through this text) reference electrode closed by a Vycor frit and dipped directly into the solution. In order to take into account the liquid junction potential between aqueous and non-aqueous solution, this electrode was calibrated with the internal reference system Fc^+/Fc, which was found at 0.46 V vs. Ag/AgCl in CH_3CN (0.53 V in dimethylformamide). The Fc^+/Fc couple (E^0 = 0.400 V vs. SHE)[53] can be used to quote potentials relative to an SHE, when needed.

Cyclic voltammograms were recorded with a EG&G PAR 273A instrument. Solution concentrations were approx. 1 mM for the catalyst and 0.1 M for the supporting electrolyte (n-Bu_4N)BF_4. Electrodes were polished with an MD-Nap polishing pad with 1-μm monocrystalline diamond DP suspension and DP lubricant blue (Struers). Additions of Et_3NHCl were made by syringe as a 50 mM solution in dimethylformamide.

Bulk electrolysis experiments and coulometry were carried out on an EG&G PAR 273A instrument in dimethylformamide, using a mercury pool cathode. The platinum-grid + carbon-foam counter electrode was placed in a separate compartment connected by a glass-frit and filled with a 0.1 M solution of ($n$$Bu_4N$)$BF_4$ in degassed dimethylformamide. A made-to-measure electrolysis cell with a cylindrical reservoir was used. The mercury pool surface was therefore identical from one experiment to another. The mercury surface was measured as 1.23 cm^2. The electrolysis cell constant was determined to be 2.34×10^{-4} s^{-1} by performing bulk electrolysis of methylviologen hexafluorophosphate.[54]

The following procedure was followed for catalytic acid reduction bulk electrolysis: A degassed dimethylformamide solution (6–10 mL) containing 0.1 M ($n$$Bu_4N$)$BF_4$ was first electrolyzed at –1.60 V vs. Ag/AgCl until the current reached 1% of its initial value. The catalyst was then added and electrolysis was also performed at –1.60 V vs. Ag/AgCl until the current reached 1% of its initial value. Et_3NHCl was then added and electrolysis was still performed at –1.60 V vs. Ag/AgCl. The faradaic yield was estimated from a periodic volumetric measurement of the amount of evolved gas. Hydrogen was tested for purity using a Delsi Nermag DN200 GC chromatograph equipped with a 3 m Porapack column and a thermal conductivity detector (TCD). Except when using $(Et_4N)_2$[Ni(emi)] as the catalyst, the electrolytic solutions remained clear after catalysis. We checked that neither the mercury pool nor the graphite electrode exhibit catalytic activity when washed after electrochemical experiments and replaced under the same conditions in the absence of catalyst. We can thus rule out the formation of any heterogeneous catalysis (coating or amalgam).

Cyclic voltammograms were simulated using the DigiElch software.[25–30] A first simulation and best-fitting was performed for **2** and $(NEt_4)_2$**4** in dimethylformamide in the absence of added acid. Parameters were refined until voltammograms recorded at 20, 50, and 100 mV s^{-1} could be simulated using the same set of values. The resulting parameters were kept unchanged for simulation of voltammograms recorded in the presence of acid. The model was then modified to include the catalytic steps and the new parameters refined until one set of values provided correct simulation of the voltammograms recorded in the presence of various amounts of added acid (1, 1.5, 3, and 10 equiv.) at different scan rates (20, 50, and 100 mV s^{-1}).

Crystal Structure Analysis: Crystallographic data are summarized in Table 2. Data collection was performed at 298 K with a Bruker SMART diffractometer with a CCD area detector, with graphite-monochromated Mo-K_α radiation (λ = 0.71073 Å). Empirical absorption correction (Sadabs) was performed. Molecular structures were solved by direct methods and refined on F^2 by full-matrix least-squares techniques with the SHELXTL package,[55] with anisotropic thermal parameters. All non-hydrogen atoms were refined anisotropically; hydrogen atoms were generally found and refined isotropically. The hydrogen atoms of the methyl and isopropyl groups of the p-cymene ligands and the solvent molecules were placed in ideal positions and refined as riding atoms with individual isotopic displacement parameters.

Table 2. Crystallographic data for **6**Cl·2$CHCl_3$ and **1**BF_4.

	6Cl·2CH_2Cl_2	**1**BF_4
Formula	$C_{29}H_{38}Cl_6RuS_2$	$C_{26}H_{38}BClF_4NiRuS_4$
Molecular mass	764.53	760.84
Color	orange	red
Crystal size [mm^3]	$0.50 \times 0.20 \times 0.20$	$0.30 \times 0.10 \times 0.05$
Crystal system	triclinic	monoclinic
Space group	$P\bar{1}$	$P2_1/n$
a [Å]	13.900 (6)	13.823(4)
b [Å]	14.225(6)	11.843(3)
c [Å]	17.531(7)	18.598(5)
α [°]	96.280(8)	90
β [°]	92.949(7)	97.029(6)
γ [°]	98.191(8)	90
V [$Å^3$]	3402(2)	3021.7(14)
Z	4	4
ρ_{calcd} [mg m^{-3}]	1.492	1.672
μ [cm^{-1}]	10.73	15.29
Reflections measured	21319	8075
Unique reflections (R_{int})	15538 (Rint = 0.0127)	4189 (Rint = 0.0251)
Refined parameters	913	514
Observed reflections [$I > 2\sigma(I)$]	13084	3596
R indices (all data)	R_1[a] = 0.0581, wR_2[b] = 0.1001	R_1 = 0. 0592, wR_2 = 0.1471
Goodness of fit (S)	1.12	1.03
$\Delta\rho$ (max/min) [e $Å^{-3}$]	1.081/–1.077	1.993/–1.711

[a] $R_1 = \Sigma||F_o| - |F_c||/\Sigma|F_o|$. [b] $wR_2 = \{\Sigma[w(F_o^2 - F_c^2)^2]/\Sigma[w(F_o^2)^2]\}^{1/2}$, $w = 1/[\sigma^2(F_o^2) + (aP)^2 + bP]$ where $P = [2F_c^2 + \max.(F_o^2, 0)]/3$ (see CIF file for values of a and b).

Crystals of **1**BF_4 were grown from a filtered solution of equimolar amounts of **1**Cl and $AgBF_4$ in chloroform with added pentane at 4 °C. The asymmetric unit contains one $\mathbf{1}^+$ cation and one BF_4^- anion disordered over two positions around the boron atom.

Crystals of **6**Cl·2CH_2Cl_2 suitable for X-ray diffraction were grown from a dichloromethane/pentane solution of **6**Cl at 4 °C. The asymmetric unit contains two $\mathbf{6}^+$ cations, two chloride anions, and four molecules of CH_2Cl_2, one of which is disordered over two positions.

CCDC-281929 (for **1**BF4) and -631503 (for **6**Cl·2$CHCl_3$) contain the supplementary crystallographic data for this paper. These data can be obtained free of charge from the Cambridge Crystallographic Data Center via ww.ccdc.cam.ac.uk/datarequest/cif.

[Ni(xbsms)Ru(*p*-cymene)Cl]Cl (1Cl): [Ru(*p*-cymene)Cl_2]$_2$ (101 mg, 0.160 mmol) and [Ni(xbsms)] (128 mg, 0.318 mmol) were dissolved in dichloromethane (5 mL). After 30 min stirring at room temperature, the mixture was evaporated to dryness. The product was passed through a silica gel column using an acetonitrile/methanol (10:1, v/v) mixture as eluent. The first fraction was dried under vacuum to yield pure **1**Cl·0.5CH_2Cl_2·2.5H_2O as a red powder (158 mg, 74%). ^{1}H NMR (300 MHz, CD_3OD): δ = 7.28 (s, 4 H, Ar), 5.73 (d, J = 5.7 Hz, 2 H, Ru-Ar), 5.54 (d, J = 5.7 Hz, 2 H, Ru-Ar), 5.33 (d, $J_{A,B}$ = 12 Hz, 2 H, ArC$H_{ax}$$H_{eq}$S), 3.87 (d, $J_{A,B}$ = 12 Hz, 2 H, ArC$H_{eq}$$H_{ax}$S), 3.02 [d, $J_{A,B}$ = 12 Hz, 2 H, $(CH_3)_2$CC$H_{eq}$$H_{ax}$], 2.51 [sept, J = 6.9 Hz, 1 H, $(CH_3)_2$CHAr], 2.50 [d, $J_{A,B}$ = 12 Hz, 2 H, $(CH_3)_2$CC$H_{eq}$$H_{ax}$], 2.12 (s, 3 H, Ru-ArC$H_3$), 1.72 (s, 6 H, Me_{ax}),1.45 (s, 6 H, Me_{eq}), 1.21 [d, J = 6.9 Hz, 6 H, $(CH_3)_2$CHAr] ppm. ESI-MS: *m*/*z* (%) 675 (100) [M]. $C_{26.5}H_{44}Cl_3NiO_{2.5}RuS_4$ (797.02): calcd. C 39.93, H 5.56, Cl 13.83, Ni 7.36, Ru 12.68, S 16.09; found C 40.19, H 5.34, Cl 12.56, Ni 7.32, Ru 11.66, S 13.21. UV/Vis: λ_{max} (ε) = 453 nm (706 $M^{-1}cm^{-1}$), 337.

(NEt$_4$)[Ni(emi)Ru(*p*-cymene)Cl] [(NEt$_4$)3]: [Ru(*p*-cymene)Cl_2]$_2$ (37.5 mg, 0.118 mmol) and $[NEt_4]_2$[Ni(emi)] (69 mg, 0.119 mmol) were dissolved in dichloromethane (5 mL). After 30 min stirring at room temperature, the mixture was evaporated to dryness. The product was extracted twice with tetrahydrofuran then pentane was added to the combined filtrates. Crystallization of this solution occurred at 4 °C. The resultant small red crystals were separated by filtration with a 71% yield (60 mg). ^{1}H NMR (300 MHz, CD_3OD): δ = 5.49 (d, J = 6 Hz, 2 H, Ru-Ar), 5.44 (d, J = 6 Hz, 2 H, Ru-Ar), 3.35 [m, 8 H, N(C$H_2$$CH_3$)$_4^+$], 2.78 [sept, J = 7.2 Hz, 1 H, $(CH_3)_2$CHAr], 2.11 (s, 3 H, Ru-ArCH_3), 1.57 (s, 4 H, NCH_2), 1.3 [m, 24 H, $(CH_3)_2$CS and N(CH_2CH_3)$_4^+$], 1.12 [d, J = 7.2 Hz, 6 H, $(CH_3)_2$CHAr] ppm. ^{13}C NMR (76 MHz, CD_3OD): δ = 85.98, 82.53 (Ar), 52.78, 52.74, 52.69 [N($CH_2$$CH_3$)$_4^+$], 32.16 or 30.57 [$(CH_3)_2$CS], 28.60 (N$CH_2$), 21.73 [$(CH_3)_2$CHAr], 17.56 [$(CH_3)_2$CHAr], 7.05 [N($CH_2$$CH_3$)$_4^+$] ppm. UV/Vis: λ_{max} (ε) = 523 nm (198 $M^{-1}cm^{-1}$), 430 (263), 353, 240.

(NEt$_4$)$_2$[Ni(emi)Ru(CO)$_2$Cl$_2$] [(NEt$_4$)$_2$4]: [Ru(CO)$_2$Cl$_2$]$_n$ (12.4 mg, 0.054 mmol) and $[NEt_4]_2$[Ni(emi)] (30 mg, 0.052 mmol) were dissolved in dichloromethane (5 mL). After 5 min stirring at room temperature, the mixture was evaporated to dryness to give a red solid. ^{1}H NMR (300 MHz, CD_3OD): δ = 3.47 [m, 16 H, N(C$H_2$$CH_3$)$_4^+$], 3.16 (s, 4 H, NC$H_2$), 1.62 [m, 12 H, $(CH_3)_2$CS], 1.38 [m, 24 H, N(CH_2CH_3)$_4^+$] ppm. IR: (CH_2Cl_2): ν_{CO} = 2037 (s), 1958 (s) cm^{-1}. UV/Vis: λ_{max} (ε) = 517 nm (185 $M^{-1}cm^{-1}$), 390–410.

[("C_3S_2")Ru(CO)$_2$Cl$_2$] (5): [Ru(CO)$_2$Cl$_2$]$_n$ (219 mg, 0.961 mmol) and 1,7-diphenyl-2,6-dithiaheptane ("C_3S_2"; 274 mg, 0.951 mmol) were dissolved in methanol (5 mL). After stirring for 1 h at room temperature, the mixture was filtered and the filtrate evaporated to dryness. The product was passed through a silica gel column using dichloromethane as eluent. The first pale-yellow fraction was dried under vacuum to yield [("C_3S_2")Ru(CO)$_2$Cl$_2$]·0.5CH_2Cl_2·0.9CH_3CN as a red powder (132 mg, 26.7%). ^{1}H NMR (300 MHz, $CDCl_3$): δ = 7.37 (m, 10 H, Ar), 4.23 (s, 4 H, PhCH_2S), 2.83 (m, 4 H, CH_2CH_2S), 2.13 (m, 2 H, C$H_2$$CH_2$S) ppm. ^{13}C NMR (76 MHz, $CDCl_3$): δ = 191.93 (CO), 130.42, 130.00, 129.72, 129.54, 129.39 (Ar), 41.77 (PhCH_2S), 28.49 ($CH_2$$CH_2$S), 24.19 ($CH_2$$CH_2$S) ppm. IR ($CH_2Cl_2$): ν_{CO} = 2074 (s), 2007 (s) cm^{-1}. $C_{21.3}H_{23.2}Cl_{2.5}N_{0.9}O_2RuS_2$ (577.66): calcd. C 44.28, H 4.04, Cl 15.34, Ru 17.49, S 11.10; found C 43.83, H 4.13, Cl 13.77, Ru 17.66, S 11.44. UV/Vis: λ_{max} (ε) = 381 nm (295 $M^{-1}cm^{-1}$).

[("C_3S_2")Ru(*p*-cymene)Cl]Cl (6Cl): [Ru(*p*-cymene)Cl_2]$_2$ (166 mg, 0.524 mmol) and "C_3S_2" (151 mg, 0.524 mmol) were dissolved in dichloromethane (5 mL). After 30 min stirring at room temperature, the mixture was evaporated to dryness. The product was then passed through a silica gel column using methanol as eluent. The first red fraction was dried under vacuum to yield [("C_3S_2")Ru(*p*-cymene)Cl]Cl·2CH_2Cl_2 (187 mg, 48%) as a red powder. ^{1}H NMR (300 MHz, CD_3OD): δ = 7.47 (m, 10 H, Ar), 5.87 (d, J = 6 Hz, 2 H, Ru-Ar), 5.71 (d, J = 6 Hz, 2 H, Ru-Ar), 4.32 (dd, $J_{A,B}$ = 12.9 Hz, ν_A = 5.36, ν_B = 5.29, 4 H, PhCH_2S), 2.8 (m, 4 H, SC$H_2$$CH_2$), 2.77 [sept, 1 H, $(CH_3)_2$CHAr], 2.32 (m, 2 H, SCH_2CH_2), 2.26 (s, 3 H, Ru-ArCH_3), 1.35 [d, J = 7.2 Hz, 6 H, $(CH_3)_2$CHAr] ppm. ^{13}C NMR (76 MHz, CD_3OD): δ = 134.77, 130.64, 129.72, 129.43, 129.20 (Ar), 88.29, 87.86 (Ru-Ar), 47–50 ($PhCH_2$S), 31.55, 30.39, 30.24, 29.70 [$(CH_3)_2$CHAr, S$CH_2$$CH_2$, $SCH_2$$CH_2$], 22.06 [$(CH_3)_2$CHAr], 17.86 (Ru-Ar$CH_3$) ppm. ESI-MS: *m*/*z* (%) 596 (100) [M]$^+$. $C_{29}H_{38}Cl_6RuS_2$ (764.53): calcd. C 45.56, H 5.01, Cl 27.82, Ru 13.22, S 8.39; found C 42.25, H 4.41, Cl 24.56, Ru 11.37, S 7.86. UV/Vis: λ_{max} (ε) = 351 nm (886 $M^{-1}cm^{-1}$), 429.

Supporting Information (see also the footnote on the first page of this article): Cyclic voltammograms of **5**, **6**Cl, and Et_3NHCl in dimethylformamide solution; cyclic voltammograms of $(Et_4N)_2$[Ni(emi)] in the presence of various amounts of Et_3NHCl in dimethylformamide solution; cyclic voltammograms and steady-state rotating-disk-electrode voltammograms recorded for (NEt$_4$)**3** and (NEt$_4$)**4** before and after catalysis and parameters used to simulate cyclic voltammograms using the mechanisms described in Schemes 2 and 3 using DigiElch 2.0.

Note Added in Proof (May 2, 2007): During correction of the proofs, the synthesis and full characterization of the bridging hydride derivative of a dinuclear complex [(L)Ni(μ-H)Ru(C_6Me_6)]$^+$ was reported by Ogo et al.[56] This species was obtained from the hydrogen reduction of a nickel-ruthenium compound very similar to $\mathbf{1}^+$ and $\mathbf{3}^-$. As this reaction corresponds to the addition of two electrons and one proton to the Ni^{II}-Ru^{II} state, this new compound is a stable analogue of the reactive intermediates proposed here in the catalytic mechanisms for hydrogen electro-production.

Acknowledgments

The authors thank Dr. Nicolas Duraffourg for performing two-dimensional NMR experiments and the Life Science Division of the CEA for financial support within the Biohydrogen program.

[1] D. J. Evans, C. J. Pickett, *Chem. Soc. Rev.* **2003**, *32*, 268–275.
[2] A. Volbeda, J. C. Fontecilla-Camps, *Dalton Trans.* **2003**, 4030–4038.
[3] Y. Nicolet, C. Piras, P. Legrand, C. E. Hatchikian, J. C. Fontecilla-Camps, *Structure Fold. Des.* **1999**, *7*, 13–23.

[4] J. W. Peters, W. N. Lanzilotta, B. J. Lemon, L. C. Seefeldt, *Science* **1998**, *282*, 1853–1858.
[5] A. Volbeda, M. H. Charon, C. Piras, E. C. Hatchikian, M. Frey, J. C. Fontecilla-Camps, *Nature* **1995**, *373*, 580–587.
[6] A. Volbeda, E. Garcin, C. Piras, A. L. de Lacey, V. M. Fernandez, E. C. Hatchikian, M. Frey, J. C. Fontecilla-Camps, *J. Am. Chem. Soc.* **1996**, *118*, 12989–12996.
[7] Y. Higuchi, H. Ogata, K. Miki, N. Yasuoka, T. Yagi, *Structure* **1999**, *7*, 549–556.
[8] A. K. Jones, E. Sillery, S. P. J. Albracht, F. A. Armstrong, *Chem. Commun.* **2002**, 866–867.
[9] M. Y. Darensbourg, E. J. Lyon, J. J. Smee, *Coord. Chem. Rev.* **2000**, *206*, 533–561.
[10] E. Bouwman, J. Reedijk, *Coord. Chem. Rev.* **2005**, *249*, 1555–1581.
[11] A. C. Marr, D. J. E. Spencer, M. Schroder, *Coord. Chem. Rev.* **2001**, *219*, 1055–1074.
[12] D. Sellmann, F. Geipel, F. Lauderbach, F. W. Heinemann, *Angew. Chem. Int. Ed.* **2002**, *41*, 632–634.
[13] J. A. W. Verhagen, M. Lutz, A. L. Spek, E. Bouwman, *Eur. J. Inorg. Chem.* **2003**, 3968–3974.
[14] Z. L. Li, Y. Ohki, K. Tatsumi, *J. Am. Chem. Soc.* **2005**, *127*, 8950–8951.
[15] D. Sellmann, F. Lauderbach, F. Geipel, F. W. Heinemann, M. Moll, *Angew. Chem. Int. Ed.* **2004**, *43*, 3141–3144.
[16] A. Perra, E. S. Davies, J. R. Hyde, Q. Wang, J. McMaster, M. Schröder, *Chem. Commun.* **2006**, 1103–1105.
[17] Y. Oudart, V. Artero, J. Pecaut, M. Fontecave, *Inorg. Chem.* **2006**, *45*, 4334–4336.
[18] J. A. W. Verhagen, D. D. Ellis, M. Lutz, A. L. Spek, E. Bouwman, *J. Chem. Soc., Dalton Trans.* **2002**, 1275–1280.
[19] H. J. Kruger, G. Peng, R. H. Holm, *Inorg. Chem.* **1991**, *30*, 734–742.
[20] W. Autenrieth, K. Wolff, *Ber. Dtsch. Chem. Ges.* **1899**, *32*, 1373.
[21] M. A. Reynolds, T. B. Rauchfuss, S. R. Wilson, *Organometallics* **2003**, *22*, 1619–1625.
[22] M. V. Rampersad, S. P. Jeffery, M. L. Golden, J. Lee, J. H. Reibenspies, D. J. Darensbourg, M. Y. Darensbourg, *J. Am. Chem. Soc.* **2005**, *127*, 17323–17334.
[23] F. A. Cotton, C. A. Kraihanzel, *Inorg. Chem.* **1963**, *2*, 533–540.
[24] S. Chardon-Noblat, A. Deronzier, R. Ziessel, D. Zsoldos, *Inorg. Chem.* **1997**, *36*, 5384–5389.
[25] M. Rudolph, *J. Electroanal. Chem.* **2003**, *543*, 23–39.
[26] M. Rudolph, *J. Electroanal. Chem.* **2003**, *558*, 171–176.
[27] M. Rudolph, *J. Electroanal. Chem.* **2004**, *571*, 289–307.
[28] M. Rudolph, *J. Comput. Chem.* **2005**, *26*, 619–632.
[29] M. Rudolph, *J. Comput. Chem.* **2005**, *26*, 633–641.
[30] M. Rudolph, *J. Comput. Chem.* **2005**, *26*, 1193–1204.
[31] V. Artero, M. Fontecave, *Coord. Chem. Rev.* **2005**, *249*, 1518–1535.
[32] W. F. Zhu, A. C. Marr, Q. Wang, F. Neese, D. J. E. Spencer, A. J. Blake, P. A. Cooke, C. Wilson, M. Schröder, *Proc. Natl. Acad. Sci. USA* **2005**, *102*, 18280–18285.
[33] M. Rousset, Y. Montet, B. Guigliarelli, N. Forget, M. Asso, P. Bertrand, J. C. Fontecilla-Camps, E. C. Hatchikian, *Proc. Natl. Acad. Sci. USA* **1998**, *95*, 11625–11630.
[34] M. C. Smith, J. E. Barclay, S. P. Cramer, S. C. Davies, W. W. Gu, D. L. Hughes, S. Longhurst, D. J. Evans, *J. Chem. Soc., Dalton Trans.* **2002**, 3410–3410.
[35] G. A. N. Felton, R. S. Glass, D. L. Lichtenberger, D. H. Evans, *Inorg. Chem.* **2006**, *45*, 9181–9184.
[36] M. Beley, J. P. Collin, R. Ruppert, J. P. Sauvage, *J. Am. Chem. Soc.* **1986**, *108*, 7461–7467.
[37] J. P. Collin, A. Jouaiti, J. P. Sauvage, *Inorg. Chem.* **1988**, *27*, 1986–1990.
[38] L. L. Efros, H. H. Thorp, G. W. Brudvig, R. H. Crabtree, *Inorg. Chem.* **1992**, *31*, 1722–1724.
[39] B. Fisher, R. Eisenberg, *J. Am. Chem. Soc.* **1980**, *102*, 7361–7363.
[40] C. J. Curtis, A. Miedaner, R. Ciancanelli, W. W. Ellis, B. C. Noll, M. R. DuBois, D. L. DuBois, *Inorg. Chem.* **2003**, *42*, 216–227.
[41] A. D. Wilson, R. H. Newell, M. J. McNevin, J. T. Muckerman, M. R. DuBois, D. L. DuBois, *J. Am. Chem. Soc.* **2006**, *128*, 358–366.
[42] T. Yamamura, S. Sakurai, H. Arai, H. Miyamae, *J. Chem. Soc., Chem. Commun.* **1993**, 1656–1658.
[43] U. T. Mueller-Westerhoff, A. Nazzal, *J. Am. Chem. Soc.* **1984**, *106*, 5381–5382.
[44] We were unfortunately unable to characterize or isolate a hydride intermediate. Reaction of the dinuclear compounds with hydride donors such as formiate, methoxide, or tetrahydroborate anions leads to intractable mixtures.
[45] V. Grass, D. Lexa, J. M. Saveant, *J. Am. Chem. Soc.* **1997**, *119*, 7526–7532.
[46] C. Baffert, V. Artero, M. Fontecave, *Inorg. Chem.* **2007**, *46*, 1817–1824.
[47] I. Bhugun, D. Lexa, J. M. Saveant, *J. Am. Chem. Soc.* **1996**, *118*, 3982–3983.
[48] M. Razavet, V. Artero, M. Fontecave, *Inorg. Chem.* **2005**, *44*, 4786–4795.
[49] M. A. Bennett, T. N. Huang, T. W. Matheson, A. K. Smith, *Inorg. Synth.* **1982**, *21*, 74–78.
[50] M. A. Bennett, A. K. Smith, *J. Chem. Soc., Dalton Trans.* **1974**, 233–241.
[51] M. J. Cleare, W. P. Griffith, *J. Chem. Soc. A* **1969**, 372.
[52] S. C. Grocott, S. B. Wild, *Inorg. Chem.* **1982**, *21*, 3535–3540.
[53] H. M. Koepp, H. Wedt, H. Strehlow, *Z. Elektrochem.* **1960**, *64*, 483.
[54] D. Plechter, *A First Course in Electrode Processes*, The Electrochemical Consultancy, Huant, UK, **1991**.
[55] G. M. Sheldrick, *SHELXTL 6.10*, 5th ed., University of Göttingen, Germany, **1994**.
[56] S. Ogo, R. Kabe, K. Uehara, B. Kure, T. Nishimura, S. C. Menon, R. Harada, S. Fukuzumi, Y. Higuchi, T. Ohhara, T. Tamada, R. Kuroki, *Science* **2007**, *316*, 585.

Received: January 19, 2007
Published Online: May 14, 2007

